Diagnosing a partly standing internal wave in Mamala Bay, Oahu

K. I. Martini,[1] M. H. Alford,[1] J. D. Nash,[2] E. Kunze,[3] and M. A. Merrifield[4]

Received 20 February 2007; revised 28 May 2007; accepted 7 June 2007; published 7 September 2007.

[1] An internal partly standing wave in Mamala Bay, Hawaii is studied using new observations and the Princeton Ocean Model (POM). Previous work suggested a convergence in the bay of east- and westbound waves emanating from Kaena Ridge and Makapuu Point, respectively. New energy flux measurements with shipboard ADCP/CTD confirm that Makapuu Point is the eastern source. After validating the POM results against observations, the model output is modally decomposed and compared with the expected theoretical patterns of kinetic and available potential energy, energy flux, and group velocity for a partly standing wave. Agreement is seen for the first baroclinic mode, which also contains most of the energy. The results confirm previous suggestions of standing wave dynamics in Mamala Bay.
Citation: Martini, K. I., M. H. Alford, J. D. Nash, E. Kunze, and M. A. Merrifield (2007), Diagnosing a partly standing internal wave in Mamala Bay, Oahu, *Geophys. Res. Lett.*, *34*, L17604, doi:10.1029/2007GL029749.

1. Introduction

[2] Two superposed free internal gravity waves of equal amplitudes, wave numbers, and frequencies travelling in opposite directions along the same axis combine to form a standing wave. Although standing internal waves are composed of converging free waves, free and standing waves have distinct properties. For each free wave, time-averaged kinetic energy (*KE*), potential energy (*PE*), and energy flux ($\overrightarrow{F}$) are spatially constant. However, for standing internal waves, the above quantities vary over a wavelength [*Nash et al.*, 2006]. Counter-intuitively, transverse fluxes oscillate sinusoidally in bands, and *KE* and *PE* have maxima occurring alternately at quarter-wavelength intervals. These patterns make standing waves much different from their component free waves. For example, misinterpretation of transverse fluxes from standing waves can result in the improper identification of internal wave sources. Thus, energy densities and fluxes must be interpreted such that standing internal waves can be distinguished from freely propagating waves. We demonstrate these concepts in the context of Mamala Bay, an embayment on the south side of the Hawaiian Island of Oahu.

[3] Mamala Bay has been the site of previous studies due to large vertical displacements (>100 m) in the bay center and large baroclinic velocities at its headlands [*Hamilton et al.*, 1995; *Eich et al.*, 2004; *Alford et al.*, 2006]. The bay (Figure 1) is situated between two energy flux sources, eastward fluxes from Kaena Ridge located on the northwestern side of Oahu (not shown) and westward fluxes thought to originate from Makapuu Point. The observed fluxes converge in Mamala Bay, consistent with elevated dissipation rates measured there [*Alford et al.*, 2006]. Output from the Princeton Ocean Model (POM) shows divergent fluxes at Makapuu Point and convergent fluxes in Mamala Bay, indicating energy sources and sinks, respectively [*Eich et al.*, 2004]. *Eich et al.* [2004] and *Alford et al.* [2006] interpreted these observations as a standing internal wave.

[4] Here, existing standing wave theory is extended to accommodate partly standing waves by allowing the convergent component waves to have unequal fluxes, as seen in Mamala Bay. Kaena Ridge is an already well-documented baroclinic internal tide generator and the western energy flux source [*Merrifield and Holloway*, 2002; *Rudnick et al.*, 2003; *Nash et al.*, 2006]. New observations taken at Makapuu Point confirm that it is the eastern generation site and the source of predominant westward fluxes into Mamala Bay. By comparing *KE*, *PE*, $\overrightarrow{F}$, and group velocity ($\overrightarrow{c_g}$) from POM model output with new theory presented here, we show the existence of a partly standing wave in Mamala Bay.

2. Data and Methods

2.1. Kaiwi Channel Shipboard Survey

[5] In February 2004, a shipboard survey measured semidiurnal energy fluxes at Makapuu Point and in Kaiwi Channel (Figure 1). The R/V *Wecoma* steamed along two lines for 25 hours each. Velocity was measured with a pair of up/downlooking 300 kHz RDI LADCPs, verified against the hull-mounted RDI 75 kHz ADCP. Temperature and salinity profiles at two stations along each line were measured every 3 hours using a Sea-Bird SBE 9 CTD. From the CTD casts, vertical displacements were calculated relative to the 25-hour temporal mean density profile.

2.2. Princeton Ocean Model

[6] A four-day run was conducted of the Princeton Ocean Model (POM) [*Blumberg and Mellor*, 1987]. POM is a three-dimensional, nonlinear, hydrostatic, free-surface, primitive-equation model. The model region includes the southeast islands in the Hawaiian Chain, but only the area surrounding Mamala Bay is considered here [*Merrifield et al.*, 2001]. Horizontal resolution is 4 km and each vertical profile is subdivided into 51 sigma levels. Stratification is from year-averaged measurements from the Hawaii Ocean

[1]Applied Physics Laboratory and School of Oceanography, University of Washington, Seattle, Washington, USA.
[2]College of Oceanic and Atmospheric Sciences, Oregon State University, Corvallis, Oregon, USA.
[3]School of Earth and Ocean Science, University of Victoria, Victoria, British Columbia, Canada.
[4]Department of Oceanography, University of Hawai'i at Manoa, Honolulu, Hawaii, USA.

0094-8276/07/2007GL029749$05.00

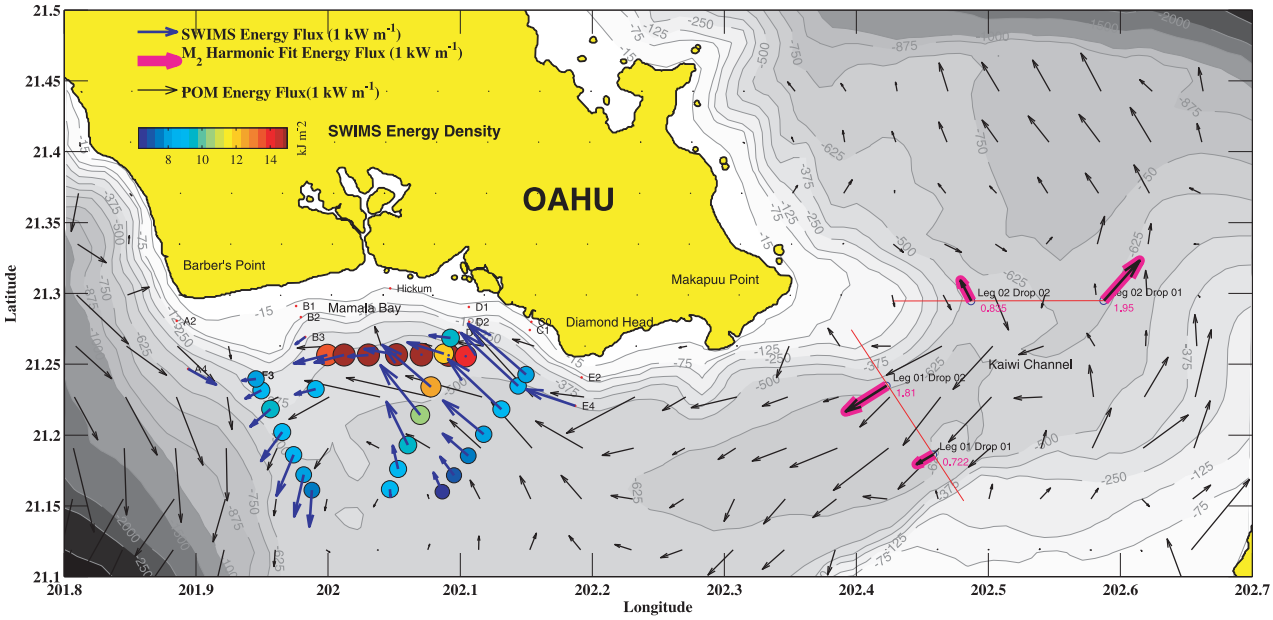

Figure 1. Depth-integrated total energy fluxes from the *Alford et al.* [2006] survey (blue), the 2004 Makapuu Point survey (pink), and POM output (black). Also shown is energy density from *Alford et al.* [2006] (colored circles), where magnitude is represented by both color and size. Makapuu Point Survey cruise tracks are shown in red.

Time Series (HOTS) and bathymetry from *Smith and Sandwell* [1997]. The model is forced along the boundaries using the M_2 tidal surface elevations from the *Egbert* [1997] global tidal model. Semidiurnal M_2 horizontal velocities and vertical displacements are extracted by harmonic analysis of the barotropic and baroclinic signals on the fourth day of the run. The model has been previously validated by *Eich et al.* [2004], against observations by *Hamilton et al.* [1995] and *Alford et al.* [2006].

2.3. Energy Density, Flux and Group Velocity

[7] Depth-integrated baroclinic energy density (E), temporally averaged over a wave period (denoted by $\langle\rangle_t$), is the sum of the horizontal kinetic energy,

$$HKE(x,y) = \frac{\rho_0}{2}\int_{-H}^{0} \langle u^2 + v^2\rangle_t \, dz, \tag{1}$$

and the available potential energy,

$$APE(x,y) = \frac{\rho_0}{2}\int_{-H}^{0} \langle N^2\zeta^2\rangle_t \, dz, \tag{2}$$

where $u(x, y, z, t)$ and $v(x, y, z, t)$ are the east- and the northward velocities, respectively, $\zeta(x, y, z, t)$ the vertical displacement, $N(z)$ the buoyancy frequency spatially averaged over the model domain, ρ_0 the average density, and $H(x, y)$ the bottom depth. For free semidiurnal waves, the ratio of HKE to APE is $(\omega^2 + f^2)/(\omega^2 - f^2) \approx 1.33$ in Mamala Bay, where f is the inertial frequency and ω the wave frequency.

[8] The depth-integrated energy flux is

$$\vec{F}(x,y) = \int_{-H}^{0} \langle \vec{u}p'\rangle_t \, dz, \tag{3}$$

where the baroclinic pressure anomaly, p', is calculated from the vertical displacements,

$$p' = \rho_o \int_{-z}^{0} N^2\zeta(z)dz - \overline{p'}, \tag{4}$$

having removed $\overline{p'} = \rho_o \frac{1}{H}\int_{-H}^{0}\int_{-z}^{0} N^2\zeta(z^*)dz^*dz$ to satisfy the baroclinic condition of zero depth average pressure perturbation [*Kunze et al.*, 2002]. For a freely propagating wave in the absence of changing stratification and geostrophic currents, HKE, APE, and $\vec{F}$ are spatially invariant.

[9] Observational estimates of group velocity,

$$\vec{c}_g^{\,calc} = \frac{\vec{F}}{E}, \tag{5}$$

are computed from depth-integrated energy density and flux [*Alford and Zhao*, 2006]. Freely propagating mode-n internal waves in a stratified ocean have a theoretical group speed,

$$|c_g^{theory}| = \left(\frac{\overline{N}H}{n\pi}\right)\frac{\sqrt{\omega^2 - f^2}}{\omega}, \tag{6}$$

where $\overline{N}$ is the depth-averaged buoyancy frequency and n the mode number [*Alford et al.*, 2006]. For a given mode, observed group speeds for standing waves are smaller than those for freely propagating waves, $|c_g^{calc}| < |c_g^{theory}|$.

[10] In a wave field composed of many modes, $|c_g^{calc}|$ can be compared to theoretical values by first decomposing the signals into normal modes. Theoretical flat-bottomed modes are calculated from the corresponding depth and stratification at each location. Depth-integrated energy density, flux and group speed are then calculated for each mode.

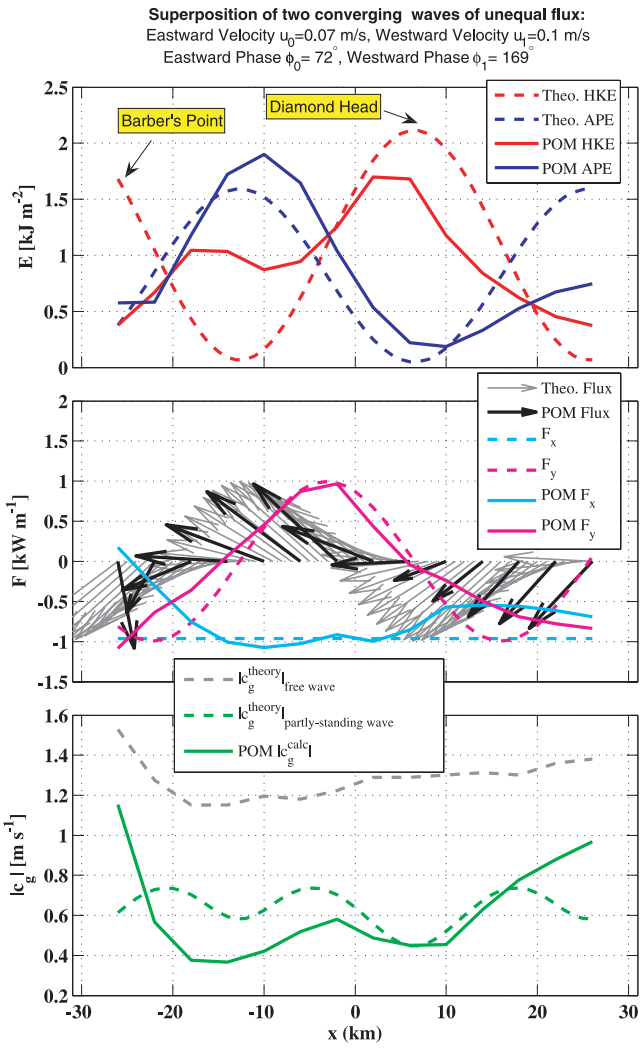

Figure 2. Expected theoretical values from the 1-D model of HKE, APE, $\overrightarrow{F}$, and $|\overrightarrow{c_g^{calc}}|$ for a partly standing mode-1 wave (dashed) are compared to a zonal slice of mode-1 values from POM (solid). Also shown is the theoretical group speed for a mode-1 free-wave (grey dashed). Grey lines in Figure 4 indicate the slice location.

2.4. Partly Standing Waves

[11] The simplest standing wave case is the superposition of two free waves with the same frequency and amplitude traveling in opposite directions. Following *Petruncio et al.* [1998] and *Nash et al.* [2004, 2006], the mode-1 standing wave *HKE*, *APE*, and $\overrightarrow{F}$ equations are generalized to include partly standing waves by using waves of unequal amplitudes. Illustrated here is a simple one-dimensional zonal partly standing wave model (Figure 2, dashed curves). Predictions from this simple theory are compared to POM output to identify partly standing wave signals in Mamala Bay.

[12] The 1-D model superposes two converging semidiurnal mode-1 waves of unequal amplitude and phase in constant stratification,

$$u = [u_0 \sin(k_x x - \omega t - \phi_0) + u_1 \sin(k_x x + \omega t - \phi_1)] \cos(k_z z), \tag{7}$$

where u_o and u_1 are the modal amplitudes of east- and westbound velocity, respectively, ϕ_0 and ϕ_1 are the east- and westbound phases, respectively, $k_z = n\pi/H$ is the vertical wave number, and $k_x = k_z\sqrt{\omega^2 - f^2}/\overline{N}$ is the horizontal wave number. The purely-standing wave case can be regained by using equal incident amplitudes.

[13] Meridional velocity, perturbation pressure, and vertical displacement are written in terms of the zonal velocity via the internal wave polarization equations. From these equations, the depth-integrated and temporally averaged kinetic and potential energies for a partly standing wave oriented along the x-axis are:

$$\langle HKE \rangle_{zt} = \frac{\rho_0}{8}\left(1 + \frac{f^2}{\omega^2}\right)\left[(u_0 - u_1)^2 + 4u_0u_1 \sin^2(k_x x - 0.5\Phi)\right] \tag{8}$$

and

$$\langle APE \rangle_{zt} = \frac{\rho_0}{8\omega^2}\frac{\omega^2 - f^2}{\overline{N}^2}\left[(u_0 - u_1)^2 + 4u_0u_1 \cos^2(k_x x - 0.5\Phi)\right], \tag{9}$$

where total phase, $\Phi = \phi_0 + \phi_1$. Both *HKE* and *APE* have alternating maxima and minima that occur at half-wavelength intervals, whose locations are determined by the incident wave phases (Figure 2 (top), dashed). Unlike a free wave, the ratio of *HKE* to *APE* is not constant, but instead varies from 0 to infinity when $u_0 = u_1$.

[14] Parallel (F_x) and transverse (F_y) energy fluxes are:

$$F_x = \langle u'p' \rangle_{zt} = \frac{\rho_0}{4}\frac{\overline{N}\sqrt{\omega^2 - f^2}}{\omega k_z}\left[u_0^2 - u_1^2\right] \tag{10}$$

and

$$F_y = \langle v'p' \rangle_{zt} = \frac{\rho_0}{2}\frac{f}{\omega}\frac{\overline{N}\sqrt{\omega^2 - f^2}}{\omega k_z}[u_0u_1] \sin(2k_x x - \Phi). \tag{11}$$

Transverse energy flux oscillates about zero at twice the spatial frequency, k_x, of the incident waves (Figure 2 (middle), dashed). The parallel flux is constant and directed in the propagation direction of the dominant constituent wave.

[15] Group speed for a partly standing wave is found by combining equations (5), (8), (9), (10), and (11). Calculated group speeds (Figure 2 (bottom), green dashed) are less than the theoretical free-wave group speed (Figure 2 (bottom), grey dashed). In contrast to purely-standing waves, partly standing waves always have non-zero group speed.

3. Results

3.1. Makapuu Point Observations

[16] The observational survey flanked the underwater ridge off Makapuu Point, extending into Kaiwi Channel (Figure 1). Observed velocities and vertical displacements are dominated by the M_2 semidiurnal tide, as indicated by close agreement between raw values and harmonic fits (Figures 3a and 3b). Corresponding along-channel (southwest) barotropic velocities and baroclinic energy fluxes from

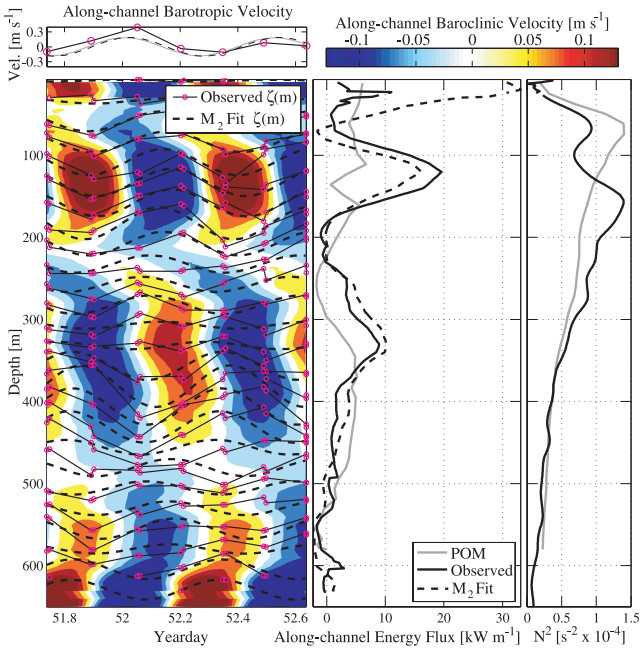

Figure 3. (a) Along-channel barotropic velocities: observed (solid black line), M_2 harmonic fit (dashed black line), and POM (solid gray line). (b) Observed baroclinic vertical displacements, ζ (solid lines) and semidiurnal fits of along-channel velocity (shading) and vertical displacement (dashed line) of the 25 hour time series at Drop 2, Leg 1 off Makapuu Point. Red circles indicate observation times. Vertical displacements are shown every 15 m. (c) POM (gray), observed (black), and M_2 harmonic fit (dashed black) along-channel energy fluxes. (d) POM (gray) and observed (black) stratification profiles.

POM and observations are similar in structure and magnitude (Figures 3a and 3c). Mean currents ($\sim$0.02 m s^{-1}) are small compared to semidiurnal baroclinic velocities ($\sim$0.1 m s^{-1}), thus horizontal advection only weakly affects observed energy fluxes (Figure 3c). In the upper water column, different stratification profiles account for energy flux discrepancies between observations and POM (Figure 3d).

[17] Observed depth-integrated semidiurnal fluxes off Makapuu Point match POM flux magnitudes and direction well at three of the drop locations (Figure 1). Both POM and observed fluxes diverge off Makapuu Point, radiating energy north into the open ocean and southeast into Mamala Bay (Figure 1). Possibly due to low horizontal resolution in the model, the flux divergence in POM occurs further to the north than observed. Nonetheless, the divergence in both the model and observations identify the ridge off Makapuu Point as the eastern generation site for waves in Mamala Bay. Over the ridge, 20–30% of the energy is contained in modes 6 and above, compared with <10% in other locations; consistent with the generation of high modes that do not propagate far from their generation site. The observed higher-mode content and divergent fluxes both indicate energy conversion from the barotropic to the baroclinic semidiurnal internal tide off Makapuu Point.

3.2. Partly Standing Waves in Mamala Bay

[18] In Mamala Bay and near the headlands, the first baroclinic mode dominates in POM (Figure 4a). Mode-1 contains at least 30% of the total energy in Mamala Bay, modes 1–2 50%, and modes 1–5 90%. Due to the dominance of the first mode it will be focused on hereafter.

[19] The theoretical mode-1 group speed for free waves (6), is dependent upon depth and mean stratification (Figure 4b). Mamala Bay is relatively flat-bottomed, so the theoretical group speed remains fairly constant. Off the Hawaiian shelf to the southwest, $|\overrightarrow{c_g^{theory}}| > 2.5$ m s^{-1}, while in Mamala Bay, $|\overrightarrow{c_g^{theory}}| \approx 1.3$ m s^{-1} (Figure 4b). Calculated mode-1 group speed (5) is approximately 0.5 m s^{-1} in Mamala Bay (Figure 4c), about 20–50% of mode-1 theoretical values (Figure 4d); indicating a standing or partly standing wave. In Kaiwi Channel and deep water southwest of Oahu, the POM mode-1 group speed approaches theoretical values, implying free propagation.

[20] Mode-1 group velocities (Figure 4d) are in the opposite direction to total energy fluxes north of Makapuu Point in POM (Figure 1). This suggests propagation of a mode-1 wave into Kaiwi Channel from an offshore source, which interferes with low mode waves emanating northward from Makapuu Point.

[21] A quantitative comparison is performed between POM and predictions from the 1-D partly standing wave model along a zonal slice through Mamala Bay's center (Figure 2). The model assumes incident waves of amplitudes 0.07 m s^{-1} and 0.1 m s^{-1}, consistent with observations [*Hamilton et al.*, 1995]. Wave phases are taken from mode-1 POM values at the headlands. Depth averaged stratification ($\overline{N}$ = 0.01 s^{-1}), depth (H = 500 m), and frequency ($\omega = M_2$) set the horizontal wavelength of the incident waves at 77 km, close to observed values [*Alford et al.*, 2006].

[22] Consistent with POM values and previous observations [*Alford et al.*, 2006], 1-D predictions yield *HKE* and *APE* maxima at the headlands and the center of Mamala Bay, respectively (Figure 2 (top)). The magnitudes and directions of parallel and transverse energy fluxes also agree well between POM and theory (Figure 2 (middle)). Overall flux is westward, due to the stronger westward incident wave. Fluxes from observations and POM turn southward westward of Makapuu Point, then northward at Diamond Head into Mamala Bay as predicted by the 1-D model. This indicates the "bowing" fluxes are the consequence of a partly standing internal wave, rather than local bathymetry.

[23] The reduction of $|\overrightarrow{c_g^{calc}}|$ relative to free wave speeds in Mamala Bay is well predicted by the 1-D model (Figure 2 (bottom)). Approaching the edges of the line, the theoretical predictions of the 1-D model diverge from POM values. This is attributed to increased meridional fluxes (eastern and western edges) and increasing depth (western only).

4. Conclusions and Discussion

[24] By extending standing wave theory to include partly standing waves and comparing this theory to new observations and output from a POM simulation, the presence of a mode-1 partly standing wave in Mamala Bay is confirmed. This new simple theory accurately reproduces patterns seen in observations and POM; specifically, 1) *APE* and *HKE*

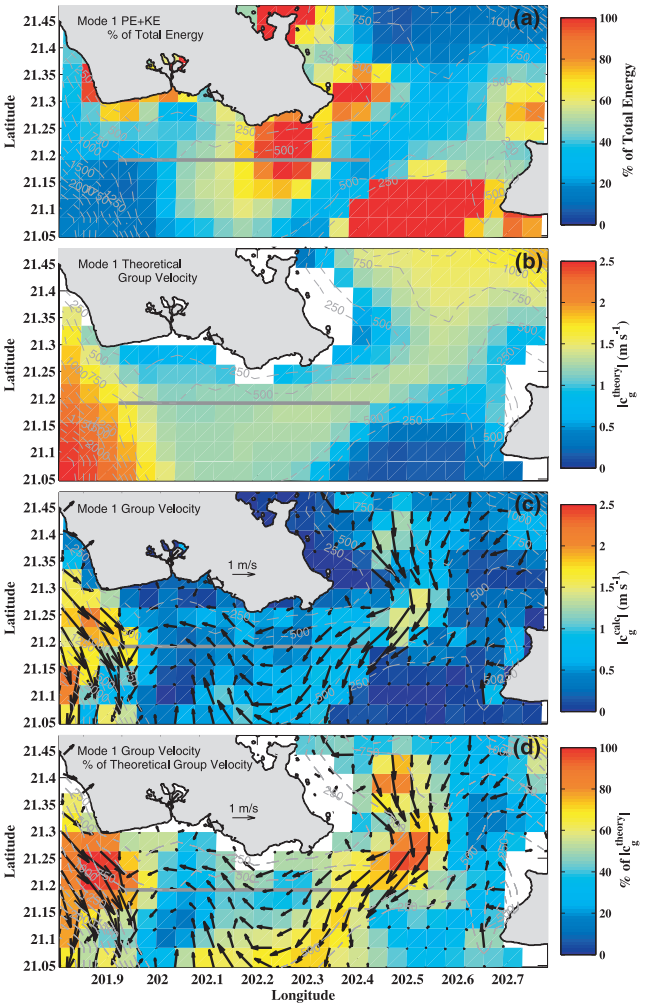

Figure 4. Maps of the first baroclinic mode from POM output. (a) Percentage of mode-1 E to the total. (b) Theoretical mode-1 group speed, $|c_g^{theo}|$, from equation (6). (c) Mode-1 $\overrightarrow{c_g}^{calc}$ (black arrows) and magnitude (shading) from equation (5). (d) The ratio of $|\overrightarrow{c_g}^{calc}|$ to $|c_g^{theo}|$. The grey line indicates the slice examined in Figure 2.

peaks in Mamala Bay and at the bay's headlands, 2) westward energy fluxes curving around Diamond Head into Mamala Bay, and 3) reduced group speed in the bay center. New observations of divergent fluxes over the ridge at Makapuu Point identify it as a source of the westward wave.

[25] Locations of *HKE*, *APE*, $\overrightarrow{F}_{transverse}$, and $|\overrightarrow{c_g}|$ peaks are sensitive to the phase of the two incident waves. Stratification modulates wave travel time and thus affects phasing [*Alford et al.*, 2006]. As a result, seasonal cycles, mesoscale eddies, or other large scale features can shift the interference pattern laterally. Energy maxima, flux convergence, and any resultant dissipation may therefore not always occur in the same location [*Hamilton et al.*, 1995; *Eich et al.*, 2004].

[26] Though formed by converging waves, standing waves themselves are not explicitly energy sinks ($\nabla \cdot \overrightarrow{F} = 0$). However, the resulting spatially variable vertical displacements and horizontal velocities create conditions favorable for increased mixing as observed by *Alford et al.* [2006]. Standing waves can be expected between adjacent sources with shared forcing mechanisms whose waves combine linearly. Examples include ridges, seamounts or submarine canyons, all of which are abundant in the ocean. Thus, standing waves may be a common occurrence. The techniques demonstrated here can be used to identify them in linear wavefields.

[27] **Acknowledgments.** This work was supported by the Office of Naval Research under grant N00014-02-1-0207. The shipboard observations were conducted while testing equipment for National Science Foundation grant OCE-0350647.

References

Alford, M. H., and Z. Zhao (2006), Global patterns of low-mode internal-wave propagation, part II: Group velocity, *J. Phys. Oceanogr.*, in press.

Alford, M. H., M. C. Gregg, and M. A. Merrifield (2006), Structure, propagation, and mixing of energetic baroclinic tides in Mamala Bay, Oahu, Hawaii, *J. Phys. Oceanogr.*, *36*, 997–1018.

Blumberg, A. F., and G. L. Mellor (1987), A description of a three-dimensional coastal ocean circulation model, in *Three-Dimensional Coastal Ocean Models*, *Coastal Estuarine Sci. Ser.*, vol. 4, edited by N. Heaps, pp. 1–16, AGU, Washington, D. C.

Egbert, G. D. (1997), Tidal data inversion: Interpolation and inference, *Prog. Oceanogr.*, *40*, 53–80.

Eich, M. L., M. A. Merrifield, and M. H. Alford (2004), Structure and variability of semidiurnal internal tides in Mamala Bay, Hawaii, *J. Geophys. Res.*, *109*(C5), C05010, doi:10.1029/2003JC002049.

Hamilton, P. J., J. Singer, and E. Waddell (1995), Mamala Bay study, ocean current measurements: A report to the Mamala Bay Commission, HI, technical report, Sci. Appl. Int. Corp., Raleigh, N. C.

Kunze, E., L. K. Rosenfeld, G. S. Carter, and M. C. Gregg (2002), Internal waves in Monterey Submarine Canyon, *J. Phys. Oceanogr.*, *32*, 1890–1913.

Merrifield, M. A., and P. E. Holloway (2002), Model estimates of M2 internal tide energetics at the Hawaiian Ridge, *J. Geophys. Res.*, *107*(C8), 3179, doi:10.1029/2001JC000996.

Merrifield, M. A., P. E. Holloway, and T. M. S. Johnston (2001), The generation of internal tides at the Hawaiian Ridge, *Geophys. Res. Lett.*, *28*, 559–562.

Nash, J., E. Kunze, J. Toole, and R. Schmitt (2004), Internal tide reflection and turbulent mixing on the continental slope, *J. Phys. Oceanogr.*, *34*, 1117–1134.

Nash, J. D., E. Kunze, C. M. Lee, and T. B. Sanford (2006), Structure of the baroclinic tide generated at Kaena Ridge, Hawaii, *J. Phys. Oceanogr.*, *36*, 1123–1135.

Petruncio, E. T., L. K. Rosenfeld, and J. D. Paduan (1998), Observations of the internal tide in Monterey Canyon, *J. Phys. Oceanogr.*, *28*, 1873–1903.

Rudnick, D., et al. (2003), From tides to mixing along the Hawaiian Ridge, *Science*, *301*, 355–357.

Smith, W. H. F., and D. T. Sandwell (1997), Global sea floor topography from satellite altimetry and ship depth soundings, *Science*, *277*, 1956–1962.

M. H. Alford and K. I. Martini, Applied Physics Laboratory, 1013 NE 40th St, Seattle, WA 98105, USA. (martini@apl.washington.edu)

E. Kunze, School of Earth and Ocean Science, University of Victoria, Victoria, BC, Canada V8W 3P6.

M. A. Merrifield, Department of Oceanography, University of Hawai'i at Manoa, Honolulu, HI 96822, USA.

J. D. Nash, College of Oceanic and Atmospheric Sciences, Oregon State University, Corvallis, OR 97331–5503, USA.